Journal of Computational Mathematics
Vol.30, No.6, 2012, 601–614.

http://www.global-sci.org/jcm
doi:10.4208/jcm.1205-m3935

INVERSE BORN SERIES FOR SCALAR WAVES*

Kimberly Kilgore Shari Moskow
Department of Mathematics, Drexel University, Philadelphia, PA 19104, USA
Email: kmk96@drexel.edu moskow@math.drexel.edu
John C. Schotland
Department of Mathematics, University of Michigan, Ann Arbor, MI, 48109, USA
Email: schotland@umich.edu

Abstract

We consider the inverse scattering problem for scalar waves. We analyze the convergence of the inverse Born series and study its use in numerical simulations for the case of a spherically-symmetric medium in two and three dimensions.

Mathematics subject classification: 78A46.
Key words: Inverse scattering.

1. Introduction

The inverse scattering problem (ISP) for scalar waves consists of recovering the spatially-varying index of refraction (or scattering potential) of a medium from measurements of the scattered field. This problem is of fundamental interest and considerable applied importance. There is a substantial body of work on the ISP that has been been comprehensively reviewed in [7–9]. In particular, much is known about theoretical aspects of the problem, especially concerning the issues of uniqueness and stability. There has also been significant effort devoted to the development of techniques for image reconstruction, including optimization, qualitative and direct methods. There is also closely related work in which small-volume expansions have been used to reconstruct the scattering properties of small inhomogeneities. The corresponding reconstruction algorithms have been implemented and their stability analyzed as a function of the signal-to-noise-ratio of the data [1–6].

In previous work, we have proposed a direct method to solve the inverse problem of optical tomography that is based on inversion of the Born series [11–13]. In this approach, the solution to the inverse problem is expressed as an explicitly computable functional of the scattering data. In combination with a spectral method for solving the linear inverse problem, the inverse Born series leads to a fast image reconstruction algorithm with analyzable convergence, stability and error.

In this paper we apply the inverse Born series to the ISP for scalar waves. We characterize the convergence, stability and approximation error of the method. We also illustrate its use in numerical simulations. We find that the series converges rapidly for low contrast objects. As the contrast is increased, the higher order terms systematically improve the reconstructions until, at sufficiently large contrast, the series diverges.

The remainder of this paper is organized as follows. In Section 2, we construct the Born series for scalar waves. We then derive various estimates that are later used to study the

* Received November 11, 2011 / Revised version received May 1, 2012 / Accepted May 4, 2012 / Published online November 16, 2012 /

convergence of the inverse Born series. The inversion of the Born series is taken up in Section 3. In Section 4, the forward operators in the Born series are calculated for the case of radially varying media. Exact solutions to the problem of scattering by spheres and annuli are discussed in Section 5. These results are used as forward scattering data for numerical reconstructions, which are shown in Section 6. Finally, our conclusions are presented in Section 7.

2. Born Series

We consider the propagation of scalar waves in $\mathbb{R}^n$ for $n \geq 2$. The field u obeys the equation

$$\nabla^2 u(x) + k^2(1 + \eta(x))u(x) = 0. \tag{2.1}$$

It will prove useful to decompose the field into the sum of an incident field and a scattered field:

$$u = u_i + u_s. \tag{2.2}$$

The incident field will be taken to be a plane wave of the form

$$u_i(x) = e^{ikx\cdot\xi} \ , \tag{2.3}$$

where k is the wave number and $\xi \in S^{n-1}$ is the direction in which the incident wave propagates. The scattered field u_s satisfies

$$\nabla^2 u_s(x) + k^2 u_s(x) = -k^2\eta(x)u(x) \tag{2.4}$$

and obeys the Sommerfeld radiation condition

$$\lim_{r\to\infty} r\left(\frac{\partial u_s}{\partial r} - iku_s\right) = 0 \ . \tag{2.5}$$

The function $\eta(x)$ is the perturbation of the squared refractive index, which is assumed to be supported in a closed ball B_a of radius a. The solution u can be expressed as the solution to the Lippmann-Schwinger integral equation

$$u(x) = u_i(x) + k^2 \int_{B_a} G(x,y)u(y)\eta(y)dy \ , \tag{2.6}$$

where the Green's function G satisfies the equation

$$\nabla_x^2 G(x,y) + k^2 G(x,y) = -\delta(x-y) \ . \tag{2.7}$$

Applying a fixed point iteration to (2.6), beginning with the incident wave, gives the well known Born series for the total field u

$$\begin{aligned} u(x) =& u_i(x) + k^2 \int_{B_a} G(x,y)\eta(y)u_i(y)dy \\ &+ k^4 \int_{B_a\times B_a} G(x,y)\eta(y)G(y,y')\eta(y')u_i(y')dydy' + \cdots . \end{aligned} \tag{2.8}$$

Let us define the scattering data

$$\phi = u_i - u. \tag{2.9}$$

The above series allows us to express this data ϕ as a power series in tensor powers of η:

$$\phi = K_1\eta + K_2\eta \otimes \eta + K_3\eta \otimes \eta \otimes \eta + \cdots . \tag{2.10}$$

The operators $\{K_j\}$ are defined as

$$\begin{aligned}(K_j f)(x_1, \xi) = -\, k^{2j} \int_{B_a \times \ldots \times B_a} & G(x_1, y_1)G(y_1, y_2)...G(y_{j-1}, y_j)\cdot \\ & \cdot u_i(y_j) f(y_1, ..., y_j) dy_1 ... dy_j,\end{aligned} \tag{2.11}$$

where x_1 is the position at which the field is measured. Note that the dependence of $K_j f$ on the incident direction ξ is made explicit. The series (2.10) will be referred to as the Born series.

In order to analyze the convergence of the Born series, we need to find bounds on the norm of the K_j operators. Assume we measure data on the boundary of a ball of radius R, ∂B_R. By proceeding with the same approach as found in [13], we find that the operators K_j are bounded in L^∞:

$$K_j : L^\infty(B_a \times \cdots \times B_a) \to L^\infty(\partial B_R \times S^{n-1}).$$

Furthermore, if we define

$$\mu_\infty = \sup_{x \in B_a} k^2 \left\| G(x, \cdot) \right\|_{L^1(B_a)}, \tag{2.12}$$

$$\nu_\infty = k^2 |B_a| \sup_{x_1 \in \partial B_R} \sup_{y \in B_a} |G(x_1, y) u_i(y)|, \tag{2.13}$$

then their operator norms satisfy the estimate

$$\left\| K_j \right\|_\infty \leq \nu_\infty \mu_\infty^{j-1}. \tag{2.14}$$

We can calculate μ_∞ explicity in three dimensions:

$$\mu_\infty = \frac{k^2}{4\pi} \int_{B_a} \frac{1}{|x|} dx = \frac{(ka)^2}{2}. \tag{2.15}$$

Here we have used the fact that the Green's function is given by

$$G(x, y) = \frac{e^{ik|x-y|}}{4\pi|x-y|}\ . \tag{2.16}$$

We calculate ν_∞ in the next section. As shown in [12] the Born series converges in the L^∞ norm when

$$\left\| \eta \right\|_{L^\infty} < \frac{2}{(ka)^2}. \tag{2.17}$$

We can similarly bound the series terms in the L^2 norm, if we view K_j as an operator defined as follows:

$$K_j : L^2(B_a \times \cdots \times B_a) \to L^2(\partial B_R \times S^{n-1}).$$

We find, again by the argument in [13], that the operator norms are bounded:

$$\left\| K_j \right\|_2 \leq \nu_2 \mu_2^{j-1}. \tag{2.18}$$

where

$$\mu_2 = \sup_{x \in B_a} k^2 \left\| G(x, \cdot) \right\|_{L^2(B_a)}, \tag{2.19}$$

$$\nu_2 = k^2 |B_a|^{\frac{1}{2}} \sup_{x_1 \in \partial B_R} \sup_{y \in B_a} \left\| G(x_1, y) u_i(y) \right\|_{L^2(\partial B_R)}. \tag{2.20}$$

3. Inverse Born Series

In the inverse scattering problem we seek to recover the coefficient η within the domain B_a from boundary measurements of the scattering data ϕ. Following [13], we express η as a formal power series in tensor powers of ϕ of the form

$$\eta = \mathcal{K}_1\phi + \mathcal{K}_2\phi \otimes \phi + \mathcal{K}_3\phi \otimes \phi \otimes \phi + \cdots, \tag{3.1}$$

where

$$\begin{aligned}
\mathcal{K}_1 &= K_1^+, \\
\mathcal{K}_2 &= -\mathcal{K}_1 K_2 \mathcal{K}_1 \otimes \mathcal{K}_1, \\
\mathcal{K}_3 &= -(\mathcal{K}_2 K_1 \otimes K_2 + \mathcal{K}_2 K_2 \otimes K_1 + \mathcal{K}_1 K_3)\mathcal{K}_1 \otimes \mathcal{K}_1 \otimes \mathcal{K}_1,
\end{aligned}$$

and for $j \geq 2$,

$$\mathcal{K}_j = -\left(\sum_{m=1}^{j-1} \mathcal{K}_m \sum_{i_1+\ldots+i_m=j} K_{i_1} \otimes \ldots \otimes K_{i_m}\right) \mathcal{K}_1 \otimes \ldots \otimes \mathcal{K}_1. \tag{3.2}$$

We will refer to equation (3.1) as the inverse Born series. We use K_1^+ to denote a regularized pseudoinverse of K_1. Since K_1 has singular values which decay to zero, it does not have a bounded inverse. The following theorem on the convergence of the inverse series was proven in [13] and improved in [10].

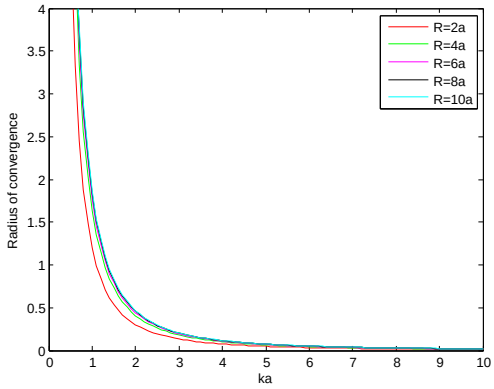

Fig. 3.1. Radius of convergence of the inverse series in the L^∞ norm for different values of R.

Theorem 3.1. *(convergence of the inverse scattering series) The inverse Born series* (3.1) *converges in the* L^∞ *norm if* $\|\mathcal{K}_1\|_p < 1/(\mu+\nu)$ *and* $\|\mathcal{K}_1\phi\|_{L^p(B_a)} < 1/(\mu+\nu)$*, where* μ *and* ν *are given by* (2.12) *and* (2.13)*. Similarly, the series converges in the* L^2 *norm if the analogous inequalities hold with* μ *and* ν *instead given by* (2.19) *and* (2.20)*. In addition, the following estimate holds for* $p = 2, \infty$

$$\left\| \tilde{\eta} - \sum_{j=1}^{N} \mathcal{K}_j\phi \otimes \cdot \otimes \phi \right\|_{L^p(B_a)} \leq C \frac{\left((\mu_p + \nu_p)\,\|\mathcal{K}_1\phi\|_{L^p(B_a)}\right)^{N+1}}{1 - (\mu_p + \nu_p)\,\|\mathcal{K}_1\phi\|_{L^p(B_a)}}, \tag{3.3}$$

where $\tilde{\eta}$ is the limit of the inverse series and $C = C(\mu_p, \nu_p, \|\mathcal{K}_1\|_p)$ does not depend on N or the data ϕ.

Remark 3.1. As shown in [13], this theorem can be extended to include convergence of the inverse series in the L^p norm for $2 \leq p \leq \infty$.

Using the Green's function (2.16) and setting the measurement radius $R = \alpha a$ for some constant α, we have that

$$\nu_\infty \leq k^2 |B_a| \frac{1}{4\pi \text{dist}(B_R, B_a)} = \frac{(ka)^2}{3(\alpha - 1)}. \tag{3.4}$$

Then the radius of convergence of the inverse series is given by

$$\frac{1}{\mu_\infty + \nu_\infty} \geq \frac{1}{\frac{(ka)^2}{3(\alpha-1)} + \frac{(ka)^2}{2}} = \frac{6(\alpha - 1)}{(ka)^2(2 + 3(\alpha - 1))}. \tag{3.5}$$

Note that as $\alpha \to \infty$,

$$\frac{1}{\mu_\infty + \nu_\infty} \to \frac{2}{(ka)^2} \ . \tag{3.6}$$

The radius of convergence as a function of ka is shown in Fig. 3.1 for various values of α. In the far field the radius is slightly bigger than in the near field.

4. Forward Operators for Radially-Varying Media

4.1. Two-dimensional problem

We now calculate explicitly the terms in the forward series for the two-dimensional case where $\Omega = \mathbb{R}^2$. We take B_R to be a disk of radius R centered at the origin such that $B_a \subset B_R$. We assume that the coefficient η depends only on the radial coordinate $r = |x|$. The fundamental solution is given by

$$G(x, y) = \frac{i}{4} H_0^{(1)}(k|x - y|), \tag{4.1}$$

which has the Bessel series expansion

$$G(x, y) = \frac{i}{4} \sum_{n=-\infty}^{\infty} e^{in(\theta_x - \theta_y)} g_n(x, y), \tag{4.2}$$

where

$$g_n(x, y) = H_n^{(1)}(kr_>) J_n(kr_<). \tag{4.3}$$

Here J_n are the Bessel functions of the first kind, $H_n^{(1)}$ are the Hankel functions, and $r_<$ and $r_>$ are defined as

$$r_< = \min(|x|, |y|), \quad r_> = \max(|x|, |y|). \tag{4.4}$$

We take u_i to be a plane wave given by

$$u_i(x) = e^{ikx \cdot \xi}, \tag{4.5}$$

which has the series expansion

$$u_i(x) = \sum_{n=-\infty}^{\infty} i^{|n|} e^{in(\theta - \theta_0)} J_{|n|}(kr), \tag{4.6}$$

where, in polar coordinates, $x = (r, \theta)$ and θ_0 is the polar angle of the unit vector ξ on S^1. The first term in the forward series is given by

$$\phi^{(1)}(\theta, \theta_0) = -k^2 \int_{B_a} G(x, x_1) u_i(x_1) \eta(x_1) dx_1. \tag{4.7}$$

If $y \in \partial B_R$, the functions g_n become

$$g_n(x, y) = \tilde{g}_n(x) = H_n(kR) J_n(kr). \tag{4.8}$$

If we introduce polar coordinates

$$x_1 = (r_1, \theta_1) \ , \tag{4.9}$$

take x to be on ∂B_R and insert the formulas (4.2), (4.8) and (4.6) into (4.7) and carry out the angular integral, we obtain

$$\phi^{(1)}(\theta, \theta_0) = -\frac{\pi i k^2}{2} \int_0^R \sum_m e^{im(\theta - \theta_0)} H_m(kR) J_m(kr_1) i^m J_m(kr_1) \eta(r_1) r_1 dr_1 \ . \tag{4.10}$$

We can therefore calculate the Fourier coefficients

$$\begin{aligned} \phi^{(1)}_{m_1, m_2} &= \int_0^{2\pi} \int_0^{2\pi} e^{-im_1\theta - im_2\theta_0} \phi^{(1)}(\theta, \theta_0) d\theta d\theta_0 \\ &= -2i^{m+1} k^2 \pi^3 H_m(kR) \int_0^R (J_m(kr_1))^2 \eta(r_1) r_1 dr_1, \end{aligned} \tag{4.11}$$

which is only nonzero when $m_1 = m_2$, so we put $m = m_1 = m_2$. We introduce a rescaling of the Fourier coefficients of the form

$$\psi^{(1)}_m = \left(\frac{1}{H_m(kR) 2\pi^3 i^{m+1}} \right) \phi^{(1)}_m. \tag{4.12}$$

Then, the first term in the series is given by

$$\psi^{(1)}_m = -k^2 \int_0^R (J_m(kr_1))^2 \eta(r_1) r_1 dr_1. \tag{4.13}$$

Repeating this process, we can calculate the second term in the forward series

$$\phi^{(2)}(\theta, \theta_0) = -k^4 \int_{B_a \times B_a} G(x, x_1) \eta(x_1) G(x_1, x_2) \eta(x_2) u_i(x_2) dx_1 dx_2. \tag{4.14}$$

As above, we rescale the Fourier coefficients

$$\begin{aligned} \psi^{(2)}_m = \frac{-ik^4 \pi}{2} \int_0^R \int_0^R & J_m(kr_1) \eta(r_1) H_m(k \max(r_1, r_2)) J_m(k \min(r_1, r_2)) \\ & \cdot \eta(r_2) J_m(kr_2) r_1 r_2 dr_1 dr_2. \end{aligned} \tag{4.15}$$

For the nth term in the series, we have the general formula

$$\begin{aligned} \psi^{(n)}_m = \frac{-i^{n+1} k^{2n} \pi^{n-1}}{2^{n-1}} \int_0^R \cdots \int_0^R & J_m(kr_1) \eta(r_1) H_m(k \max(r_1, r_2)) \\ & \cdot J_m(k \min(r_1, r_2)) \cdot \eta(r_2) \cdots H_m(k \max(r_{n-1}, r_n)) J_m(k \min(r_{n-1}, r_n)) \\ & \cdot \eta(r_n) J_m(kr_n) r_1 \cdots r_n dr_1 \cdots dr_n. \end{aligned} \tag{4.16}$$

4.2. Three-dimensional problem

The setup here is strictly analogous to that of the two-dimensional case. The Green's function is given by (2.16) and is expressible as the series expansion

$$G(x,y) = ik\sum_{l=0}^{\infty}\sum_{m=-l}^{l} g_l(x,y)Y_{lm}(\hat{x})Y_{lm}^*(\hat{y}), \tag{4.17}$$

where

$$g_l(x,y) = h_l^{(1)}(kr_>)j_l(kr_<). \tag{4.18}$$

Here j_l are the spherical Bessel functions and $h_l^{(1)}$ are the spherical Hankel functions of the first kind. If $y \in \partial B_R$, g_l takes the form

$$g_l(x,y) = \tilde{g}_l(x) = h_l^{(1)}(kR)j_l(kr). \tag{4.19}$$

If the incident wave, u_i is a plane wave as in the two dimensional case, then u_i has the series expansion

$$u_i(x) = 4\pi\sum_{l,m} i^l j_l(kr)Y_{lm}(\hat{x})Y_{lm}^*(\xi). \tag{4.20}$$

Introducing spherical coordinates with $x \in \partial B_R$

$$x_1 = (r_1, \hat{x_1}) \text{ and } x = (R, \hat{x}), \tag{4.21}$$

and making use of (4.17), (4.19) and (4.20), we obtain

$$\begin{aligned}\phi^{(1)}(\hat{x},\xi) &= -k^2\int_{B_a} G(x,x_1)u_i(x_1)\eta(x_1)dx_1 \\ &= -4\pi ik^3\int_0^R \sum_{l,m} Y_{lm}(\hat{x})\tilde{g}_l(r_1)i^l j_l(kr_1)Y_{lm}^*(\xi)\eta(r_1)r_1^2 dr_1\ .\end{aligned} \tag{4.22}$$

Now, taking the Fourier transform we have

$$\begin{aligned}\phi^{(1)}_{l_1,m_1,l_2,m_2} &= \int_{S^2}\int_{S^2} Y_{l_1m_1}^*(\hat{x})Y_{l_2m_2}(\xi)\phi^{(1)}(\hat{x},\xi)d\hat{x}d\xi \\ &= -4\pi ik^3\delta_{l_1l_2}\int_0^R \tilde{g}_{l_1}(r_1)i^{l_1}j_{l_1}(kr_1)\eta(r_1)r_1^2 dr_1.\end{aligned} \tag{4.23}$$

Since the right hand side no longer depends on m_1 and m_2, we define $l = l_1 = l_2$ so that

$$\phi_l^{(1)} = -4\pi k^3 i^{l+1}h_l^{(1)}(kR)\int_0^R (j_l(kr_1))^2\eta(r_1)r_1^2 dr_1. \tag{4.24}$$

As in the two dimensional case, we can repeat this process for higher order terms, and find the following generalized form for the nth term in the series:

$$\begin{aligned}\phi_l^{(n)} = -4\pi k^{3n}i^{l+n}h_l^{(1)}(kR)\int_0^R\cdots\int_0^R & j_l(kr_1)\eta(r_1)h_l^{(1)}(k\max(r_1,r_2)) \\ & \cdot j_l(k\min(r_1,r_2))\eta(r_2)\cdots h_l^{(1)}(k\max(r_{n-1},r_n))j_l(k\min(r_{n-1},r_n)) \\ & \cdot \eta(r_n)j_m(kr_n)r_1^2\cdots r_n^2 dr_1\cdots dr_n.\end{aligned} \tag{4.25}$$

5. Exact Solutions for Spheres and Annuli

5.1. Spherical scatterer

For the problem of a ball shaped scatterer centered at the origin, the coefficient η is given by

$$\eta(r) = \begin{cases} \eta_1 & 0 < r \leq R_1, \\ 0 & R_1 < r. \end{cases} \tag{5.1}$$

The solution will then be computed on two subdomains. The first is the inner disk or sphere

$$B = \{x \mid \quad |x| \leq R_1\}, \tag{5.2}$$

the second is the exterior domain. The system of equations corresponding to (2.1) with appropriate interface matching conditions is given by:

$$\nabla^2 u_1 + k_1^2 u_1 = 0 \text{ in } B, \tag{5.3a}$$

$$\nabla^2 u_2 + k^2 u_2 = 0 \text{ in } \mathbb{R}^n \setminus \overline{B}, \tag{5.3b}$$

$$u_1 = u_2 \text{ on } \partial B, \tag{5.3c}$$

$$\frac{\partial u_1}{\partial \nu} = \frac{\partial u_2}{\partial \nu} \text{ on } \partial B, \tag{5.3d}$$

where $k_1^2 = k^2(1 + \eta_1)$ is the coefficient in the inner region.

5.1.1. Disk in two dimensions

We use the Bessel series expansion (4.6) for the incident wave u_i where θ_0 is the polar angle of the incident direction ξ. We express the solution to (5.3) in a Bessel series expansion,

$$u_1(x) = \sum_{n=0}^{\infty} a_n e^{in(\theta-\theta_0)} J_n(k_1 r), \tag{5.4}$$

$$u_2(x) = u_i(x) + \sum_{n=0}^{\infty} b_n e^{in(\theta-\theta_0)} H_n(kr). \tag{5.5}$$

Applying the interface conditions allows us to obtain the following system to solve for the coefficients $\{a_n, b_n\}$:

$$\begin{bmatrix} J_n(k_1 R_1) & -H_n(kR_1) \\ k_1 J_n'(k_1 R_1) & -kH_n'(kR_1) \end{bmatrix} \begin{bmatrix} a_n \\ b_n \end{bmatrix} = i^{|n|} \begin{bmatrix} J_{|n|}(kR_1) \\ kJ_{|n|}'(kR_1) \end{bmatrix}. \tag{5.6}$$

We thus obtain an expression for ϕ for $x \in \partial B_R$:

$$\phi(\theta_0, \theta) = -\sum_{n=-\infty}^{\infty} e^{in(\theta-\theta_0)} b_n H_n(kR). \tag{5.7}$$

Computing its Fourier coefficients gives

$$\begin{aligned} \phi_{m,n} &= \int_0^{2\pi} \int_0^{2\pi} e^{-im\theta_1} e^{-in\theta_2} \phi(\theta_1, \theta_2) d\theta_1 d\theta_2 \\ &= -(2\pi)^2 \delta_{m,-n} b_{-m} H_m(kR)(-1)^m. \end{aligned} \tag{5.8}$$

Using the fact that the above expression is independent of n we can define

$$\phi_m = \phi_{m,-m} = -(2\pi)^2 b_{-m} H_m(kR)(-1)^m. \tag{5.9}$$

Using the same rescaling as in equation (4.12) gives

$$\psi_m = \left(\frac{1}{H_m(kR)2\pi^3 i^{m+1}}\right)\phi_m = -\frac{2b_{-m}(-1)^m}{\pi i^{m+1}}. \tag{5.10}$$

5.1.2. Sphere in three dimensions

In the three-dimensional case, the incident wave u_i has the Bessel series expansion (4.20). The solution to the system (5.3) can be expressed as

$$u_1(x) = \sum_{l,m} a_{lm} j_l(k_1 r) Y_{lm}(\hat{x}) Y^*_{lm}(\xi), \tag{5.11}$$

$$u_2(x) = u_i(x) + \sum_{l,m} b_{lm} h^{(1)}_l(kr) Y_{lm}(\hat{x}) Y^*_{lm}(\xi). \tag{5.12}$$

After applying the interface boundary conditions, we obtain a system of equations to solve for the coefficients $\{a_{lm}, b_{lm}\}$:

$$\begin{bmatrix} j_l(k_1R_1) & -h^{(1)}_l(kR_1) \\ k_1 j_l^{'}(k_1R_1) & -k(h^{(1)}_l)^{'}(kR_1) \end{bmatrix} \begin{bmatrix} a_{lm} \\ b_{lm} \end{bmatrix} = 4\pi i^l \begin{bmatrix} j_l(kR_1) \\ k j_l^{'}(kR_1) \end{bmatrix}. \tag{5.13}$$

Now, substituting in $x \in \partial B_R$ we get a formula for the data function

$$\phi(\xi, \hat{x}) = -\sum_{m,l} b_{lm} h^{(1)}_l(kr) Y_{lm}(\hat{x}) Y^*_{lm}(\xi). \tag{5.14}$$

We can compute its Fourier coefficients

$$\begin{aligned} \phi^{l_2 m_2}_{l_1 m_1} &= \int_{S^2 \times S^2} Y_{l_1 m_1}(\hat{x_1}) Y^*_{l_2 m_2}(\hat{x_2}) \phi(\hat{x_1}, \hat{x_2}) d\hat{x_1} d\hat{x_2} \\ &= -\delta_{l_1, l_2} \delta_{m_1, m_2} b_{l_1 m_1} h^{(1)}_{l_1}(kR) \end{aligned} \tag{5.15}$$

and, as before, define

$$\phi_m = \phi^{m m_2}_{m m_1} = -b_m h^{(1)}_m(kR). \tag{5.16}$$

5.2. Annular scatterer

The coefficient η is now assumed to be of the form

$$\eta(r) = \begin{cases} 0 & 0 < r \le R_1, \\ \eta_1 & R_1 < r \le R_2, \\ 0 & R_2 < r. \end{cases} \tag{5.17}$$

The domain is then divided into three subdomains. The first is the inner disk or sphere

$$B = \{x \mid |x| \le R_1\}, \tag{5.18}$$

the second is the middle annulus

$$A = \{x \mid R_1 < |x| \leq R_2\}, \tag{5.19}$$

and the third is the exterior region. The system of equations corresponding to (2.1) with interface matching conditions is given by:

$$\nabla^2 u_1 + k^2 u_1 = 0 \text{ in } B, \tag{5.20a}$$
$$\nabla^2 u_2 + k_1^2 u_2 = 0 \text{ in } A, \tag{5.20b}$$
$$\nabla^2 u_3 + k^2 u_3 = 0 \text{ in } \mathbb{R}^n \setminus (B \cup A), \tag{5.20c}$$
$$u_1 = u_2 \text{ on } \partial B, \tag{5.20d}$$
$$\frac{\partial u_1}{\partial \nu} = \frac{\partial u_2}{\partial \nu} \text{ on } \partial B, \tag{5.20e}$$
$$u_2 = u_3 \text{ on } (\partial A)^+, \tag{5.20f}$$
$$\frac{\partial u_2}{\partial \nu} = \frac{\partial u_3}{\partial \nu} \text{ on } (\partial A)^+, \tag{5.20g}$$

where $(\partial A)^+$ is the outer boundary of A, and $k_1^2 = k^2(1 + \eta_1)$ is the coefficient in the middle annulus.

5.2.1. Annulus in two dimensions

The incident wave u_i is given above in (4.6). The solution to (5.20) can be expressed as

$$u_1(x) = \sum_{n=-\infty}^{\infty} a_n J_n(kr) e^{in(\theta-\theta_0)}, \tag{5.21a}$$
$$u_2(x) = \sum_{n=-\infty}^{\infty} b_n J_n(k_1 r) e^{in(\theta-\theta_0)} + c_n H_n(k_1 r) e^{in(\theta-\theta_0)}, \tag{5.21b}$$
$$u_3(x) = u_i(x) + \sum_{n=-\infty}^{\infty} d_n H_n(kr) e^{in(\theta-\theta_0)}. \tag{5.21c}$$

After applying the interface boundary conditions, we obtain the following system of equations which can be solved for the four coefficients $\{a_n, b_n, c_n, d_n\}$:

$$\begin{bmatrix} J_n(kR_1) & -J_n(k_1R_1) & -H_n(k_1R_1) & 0 \\ 0 & J_n(k_1R_2) & H_n(k_1R_2) & -H_n(kR_2) \\ kJ_n'(kR_1) & -k_1J_n'(k_1R_1) & -k_1H_n'(k_1R_1) & 0 \\ 0 & k_1J_n'(k_1R_2) & k_1H_n'(k_1R_2) & -kH_n'(kR_2) \end{bmatrix} \begin{bmatrix} a_n \\ b_n \\ c_n \\ d_n \end{bmatrix}$$
$$= i^{|n|} \begin{bmatrix} -J_{|n|}(kR_1) \\ J_{|n|}(kR_2) \\ -kJ_{|n|}'(kR_1) \\ J_{|n|}'(kR_2) \end{bmatrix}. \tag{5.22}$$

The exact solution has the form:

$$\psi_m = -\frac{2d_{-m}(-1)^m}{\pi i^{m+1}}. \tag{5.23}$$

5.2.2. Annulus in three dimensions

Using the expansion of the incident wave (4.20), the solution to the three dimensional annulus problem can be expressed as

$$u_1(x) = \sum_{l,m} a_{lm} j_l(kr) Y_{lm}(\hat{x}) Y^*_{lm}(\xi), \tag{5.24a}$$

$$u_2(x) = \sum_{l,m} b_{lm} h^{(1)}_l(k_1 r) Y_{lm}(\hat{x}) Y^*_{lm}(\xi) + c_{lm} j_l(k_1 r) Y_{lm}(\hat{x}) Y^*_{lm}(\xi), \tag{5.24b}$$

$$u_3(x) = u_i(x) + \sum_{l,m} d_{lm} h^{(1)}_l(kr) Y_{lm}(\hat{x}) Y^*_{lm}(\xi). \tag{5.24c}$$

In this case, applying the interface boundary conditions, we have the following system of equations which can be solved for the four coefficients $\{a_{lm}, b_{lm}, c_{lm}, d_{lm}\}$:

$$\begin{bmatrix} j_l(kR_1) & -h^{(1)}_l(k_1R_1) & -j_l(k_1R_1) & 0 \\ 0 & h^{(1)}_l(k_1R_2) & j_l(k_1R_2) & -h^{(1)}_l(kR_2) \\ kj_l^{'}(kR_1) & -k_1(h^{(1)}_l)^{'}(k_1R_1) & -k_1 j_l^{'}(k_1R_1) & 0 \\ 0 & k_1(h^{(1)}_l)^{'}(k_1R_2) & k_1 j_l^{'}(k_1R_2) & -k(h^{(1)}_l)^{'}(kR_2) \end{bmatrix} \begin{bmatrix} a_{lm} \\ b_{lm} \\ c_{lm} \\ d_{lm} \end{bmatrix}$$
$$= 4\pi i^l \begin{bmatrix} -j_l(kR_1) \\ j_l(kR_2) \\ -kj_l^{'}(kR_1) \\ j_l^{'}(kR_2) \end{bmatrix}. \tag{5.25}$$

Again, we can define

$$\phi_m = -d_m h_m(kR). \tag{5.26}$$

6. Numerical Results

We now present the results of numerical reconstructions for the four model systems we have discussed. When computing the terms of the inverse series, we use recursion to implement the formula (3.2). The scattering data is computed from the formulas (5.10),(5.23),(5.16) and (5.26). The forward operators are implemented using the formulas (4.16) and (4.25) . We compute the pseudo-inverse $\mathcal{K}_1 = K_1^+$ by using MATLAB's built-in singular value decomposition. Since the singular values of K_1 are exponentially small, we set the recipricals of all but the largest $M = 6$ singular values to zero. When computing the data (4.16) and (4.25) we use $m = 40$ modes and discretize the integral operators on a spatial grid of 40 uniformly-spaced nodes in the radial direction. We found that increasing the number of modes and spatial grid points did not significantly change the reconstructions.

Fig. 6.1 shows reconstructions for low contrast with measurements in the near-field. In each case, five terms in the inverse series are computed. We also show the projection of η onto the subspace generated by the first M singular vectors, which gives a sense for what can be reconstructed at low frequencies, for a particular regularization. Note that the series appears to converge quite rapidly to a reconstruction that is close to the projection. As the contrast is increased, as shown in Fig. 6.2, the higher order terms lead to significant improvements compared to the linear reconstructions.

In Fig. 6.3 we present reconstructions for the high contrast case, but with measurements carried out in the intermediate field. In this situation we make use of $M = 10$ modes. Finally,

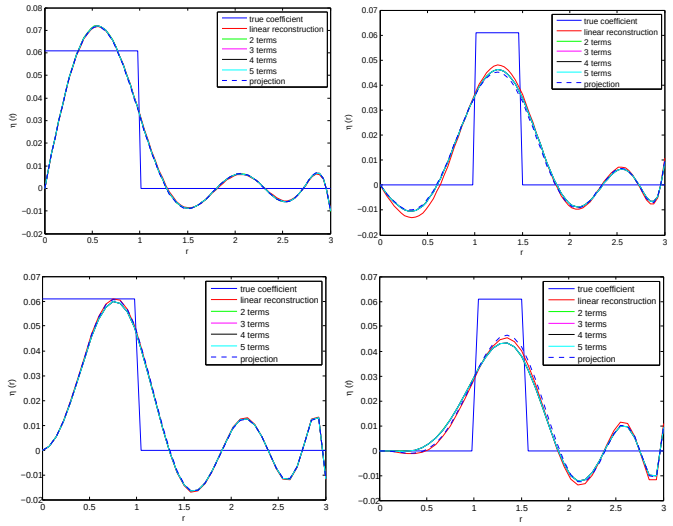

Fig. 6.1. Numerical results for small contrast measured in the near field. From top left: two dimensional disk, two dimensional annulus, three dimensional sphere, and three dimensional annulus. Here $k_1 = 1.03$, $k = 1$, $R_1 = 1$, $R_2 = 1.5$ (for annulus), and measurements are at $R = 3$. We take 6 modes in the regularized pseudoinverse K_1^+.

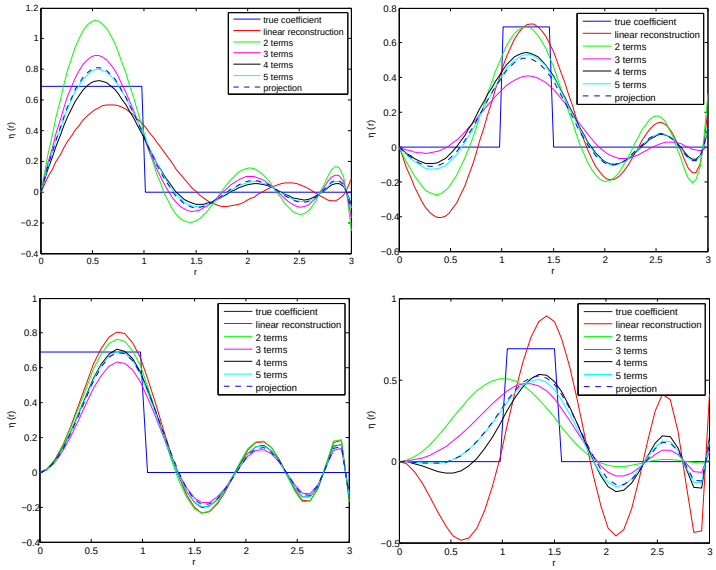

Fig. 6.2. Numerical reconstructions for larger contrast measured in the near field. From top left: two dimensional disk, two dimensional annulus, three dimensional sphere, and three dimensional annulus. Here $k_1 = 1.3$, $k = 1$, $R_1 = 1$, $R_2 = 1.5$ (for annulus), and measurements are at $R = 3$. We take 6 modes in the regularized pseudoinverse K_1^+.

in Fig. 6.4 we show reconstructions of the high contrast case with measurements in the far field using $M = 15$ modes. In both cases, the results are comparable to the near-field reconstructions shown in Fig. 6.2.

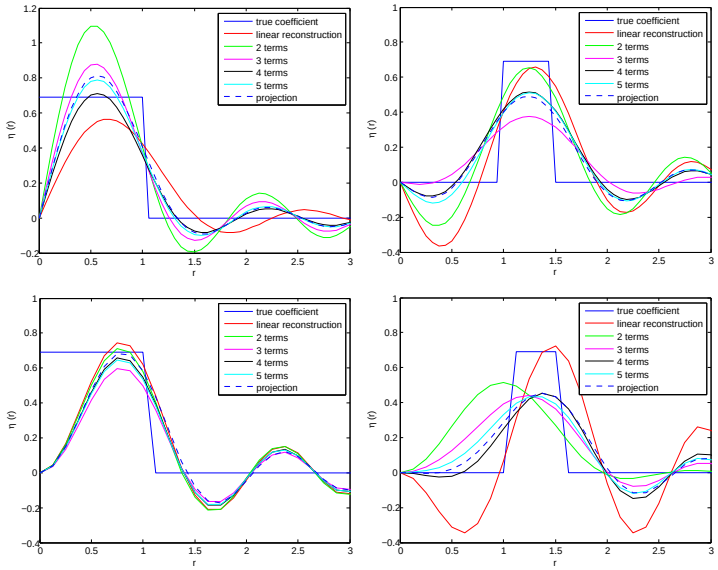

Fig. 6.3. Numerical reconstructions for larger contrast measured in the intermediate field. From top left: two dimensional disk, two dimensional annulus, three dimensional sphere, and three dimensional annulus. Here $k_1 = 1.3$, $k = 1$, $R_1 = 1$, $R_2 = 1.5$ (for annulus), and measurements are at $R = 5$. We take 10 modes in the regularized pseudoinverse K_1^+.

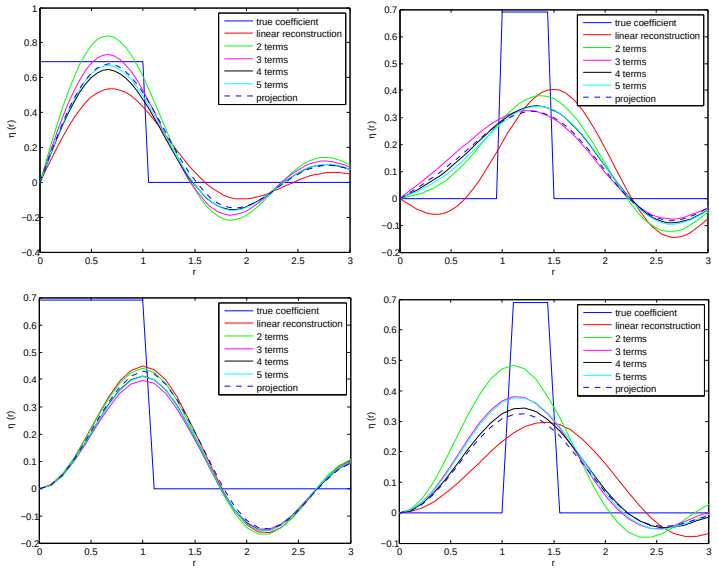

Fig. 6.4. Numerical reconstructions for larger contrast measured in the far field. From top left: two dimensional disk, two dimensional annulus, three dimensional sphere, and three dimensional annulus. Here $k_1 = 1.3$, $k = 1$, $R_1 = 1$, $R_2 = 1.5$ (for annulus), and measurements are at $R = 10$. We take 15 modes in the regularized pseudoinverse K_1^+.

7. Discussion

In conclusion, we have studied numerically the convergence of the inverse Born series for scalar waves. Exact solutions to the forward problem were used as scattering data and recon-

structions were computed to fifth order in the inverse series. We found that the series appears to converge quite rapidly for low contrast objects in both two and three dimensions. As the contrast is increased, the higher order terms systematically improve the reconstructions. We note that the results at high contrast in both the near, intermediate and far fields are qualitatively similar. We do not expect that this observation will hold up in the case of electromagnetic scattering since solutions to the Maxwell equations in the near field decay more rapidly than in the far zone.

Acknowledgments. Shari Moskow and Kimberly Kilgore were supported by the NSF grant DMS—1108858. John Schotland's work was supported by the NSF grants DMR–1120923, DMS–1115574 and DMS–1108969.

References

[1] H. Ammari and H. Kang, Reconstruction of Small Inhomogeneities from Boundary Measurements, Lecture Notes in Mathematics, 1846. Springer-Verlag, Berlin, 2004.

[2] H. Ammari and H. Kang, Polarization and Moment Tensors: with Applications to Inverse Problems and Effective Medium Theory, vol. 162, Springer-Verlag, 2007.

[3] H. Ammari and H. Kang, High-order terms in the asymptotic expansions of the steady-state voltage potentials in the presence of conductivity inhomogeneities of small diameter, *SIAM J. Math. Anal.*, **34** (2003), 1152–1166.

[4] H. Ammari and H. Kang, Boundary layer techniques for solving the Helmholtz equation in the presence of small inhomogeneities, *J. Math. Anal. Appl.,* **296**:1, (2004), 190-208.

[5] H. Ammari, H. Kang, M. Lim, and H. Zribi, The generalized polarization tensors for resolved imaging. Part I: Shape reconstruction of a conductivity inclusion, *Math. Comp.*, **81** (2012), 367–386.

[6] H. Ammari, H. Kang, E. Kim, and J.-Y. Lee, The generalized polarization tensors for resolved imaging. Part II: Shape and electromagnetic parameters reconstruction of an electromagnetic inclusion from multistatic measurements, *Math. Comp.*, **81** (2012), 839–860.

[7] Chadan, K. and Sabatier, P., Inverse Problems in Quantum Scattering Theory, Springer, 1989.

[8] Colton, D. and Kress, R., Inverse Acoustic and Electromagnetic Scattering Theory, Springer, 1992.

[9] Cakoni, F. and Colton, D., Qualitative Methods in Inverse Scattering Theory: An Introduction, Springer, 2005.

[10] Kilgore, K., Moskow, S. and Schotland, J. C., Inverse Born series for diffuse waves., *Imaging microstructures*, 113-122, Contemp. Math., 494, *Amer. Math. Soc., Providence, RI*, (2009).

[11] Markel, V., O'Sullivan, J. and Schotland, J. C., Inverse problem in optical diffusion tomography. IV. Nonlinear inversion formulas, *J. Opt. Soc. Am. A*, **30**, (2003), 903-912.

[12] Moskow, S. and Schotland, J.C., Numerical studies of the inverse born series for diffuse waves, *Inverse Problems,* **25** (2009) 095007-25.

[13] Moskow, S. and Schotland, J.C., Convergence and stability of the inverse scattering series for diffuse waves, *Inverse Problems,* **24** (2008) 065005-21.